## PAPER

Check for updates

# A simple method for floating graphene oxide films facilitates nanoscale investigations of ion and water adsorption†

Raju R. Kumal, [ID] ‡ Amanda J. Carr and Ahmet Uysal [ID] *

Graphene oxide (GO) is a promising material for separations. Nanoscale GO thin films at the air/water interface are excellent experimental models to understand molecular-scale interactions of ions and water with GO. However, the characteristics of GO, such as functional groups and flake size, also affect the thin film properties making it difficult to make systematic studies with GO thin films. This paper reports a simple, reliable, and quick method of preparing ultra-thin GO films, irrespective of their origin, and demonstrates the new opportunities possible with the utilization of this method. The total amount of GO used to form the thin film is significantly less compared to previous examples in the literature, minimizing the dissolved GO in the subphase. X-ray reflectivity (XR) studies show that the majority of the GO film has 1.5 nm thickness over a macroscopic area (∼100 cm$^2$) with very small roughness. Sum frequency generation (SFG) spectroscopy measurements show that H$_2$O and D$_2$O interact differently with GO films, a property that was not observed before. SFG data show that functional groups vary significantly between different commercially available GO samples. The differences are also characterized with XR at high resolution. X-ray fluorescence near total reflection (XFNTR) measurements show that these differences strongly affect ion adsorption and interfacial water behavior near GO, which are vital properties in separation applications. The results pave the way for future studies to elucidate the complex separation mechanisms with GO.

## 1 Introduction

Graphene oxide (GO) is a promising separation material because it combines molecular sieving with high water permeation.[1–10] The hydrophobic and hydrophilic patches on GO and their molecular-scale distribution can significantly alter mass transport.[11,12] However, direct observation of water structure near GO surfaces is very difficult in real membrane applications. Therefore, large area, ultra-thin GO films with thicknesses of only a few nanometers are vital model systems that can be easily compared to computational studies.[13,14] The amphiphilic nature of GO has been exploited to create Langmuir films at the air/water interface.[15–20] These films can be transferred on solid substrates or studied directly at the liquid surface. Drop-cast approach has been also utilized to fabricate GO membrane with controllable thickness.[21,22] However, there

are multiple factors that affect GO thin film formation that are often overlooked, which leads to inconsistencies between reported studies. First, the chemical composition of the GO, including the number and types of functional groups as well as the flake size distribution, strongly depends on the specific synthetic procedure. Standardized method of GO synthesis and characterization procedure is required to reduce the variabilities and maximize the efficiency for industrial applications.[23] Second, thin films are created at the air/water interface by preparing and spreading a dilute solution of GO (typically in a methanol/water mixture). This paper introduces a simple and effective spreading process. The prepared films are high quality, *i.e.* homogeneous across macro dimensions and smooth, and can be examined with surface-specific probes to reveal molecular-scale details including information about ion adsorption and interfacial water structure.

GO does not readily form a Langmuir monolayer in contrast to some commonly studied lipids with distinct hydrophobic tails and hydrophilic heads. Therefore, during the Langmuir film formation a significant amount of GO can dissolve in the water subphase leaving only a small amount of material to form the thin film at the interface. Dissolution of GO in the subphase has been acknowledged since early investigations.[15] To promote interfacial film formation, studies have suggested options such as sonicating the GO spreading solution to disperse flakes,[24]

*Chemical Sciences and Engineering Division, Argonne National Laboratory, Lemont, IL 60439, USA. E-mail: ahmet@anl.gov; Web: https://www.anl.gov/profile/ahmet-uysal*

† Electronic supplementary information (ESI) available: Experimental details of SFG and synchrotron experiments, XPS characterization of GO films, additional SFG data on D$_2$O subphase, zoomed in version of Fig. 2c, and fit parameters of SFG and XR data analysis. See DOI: https://doi.org/10.1039/d3ra07254a

‡ Present Address: Fresenius Kabi USA, 2020 N. Ruby Street, Melrose Park, IL 60160, USA.

introducing additional surfactants,[25] bubbling nitrogen through the subphase to transport GO flakes to the surface,[26] or decreasing the droplet size of the GO spreading solution through electro-spraying.[27] Surface energy calculations suggested that a balance between hydrophobicity and hydrophilicity corresponding to 46° contact angle is ideal for forming GO films at the oil water interface.[28] Electro-spraying and bubbling methods require additional equipment. All of these methods also utilized large volumes of the GO spreading solution (typically 1–10 mL of 0.2 mg mL$^{-1}$ GO solution) to create ∼100 cm$^2$ thin films. Spreading these large volumes *via* dropwise addition on a subphase can take up to 30 minutes.

Several studies have focused on the *in situ* characterization of GO films at the air/water interface. Bonatout *et al.* used X-ray reflectivity (XR) and suggested a bilayer structure for GO sheets with water molecule bridges.[24] This study did not report the amount of spreading solution used. The maximum momentum transfer, $q_{max}$, for XR data was 0.35 Å$^{-1}$, which suggests a rough surface and limits their resolution to $\frac{\pi}{q_{max}} \tilde{9}$Å. The study also did not show the calculated electron density profiles from the XR fits but reported the fit parameters for a two-layer model, which suggests a 2 nm total thickness for the GO film. López-Díaz *et al.* used neutron reflectivity (NR) to show that the oxidative debris can form an extra layer underneath GO films.[29] However, the presence of oxidative debris has been contested by several studies.[30,31] They used a two-layer model to fit the NR data, with 2 nm GO and 1 nm impurity layer. The purified samples showed a single 2 nm GO layer. This study used 2.5 mL of spreading solution. The $q_{max}$ of NR data was 0.2 Å$^{-1}$, meaning their resolution was 16 Å. These studies only focused on the GO structure and did not investigate ion or water interactions with the GO film. Hong *et al.* studied the structure of water near GO using vibrational sum frequency generation (VSFG) spectroscopy.[17] They used 1.1 mL spreading solution. VSFG does not provide direct structural information about the GO films. Instead, it provides the structure of interfacial water and its response to the salts in the subphase.[17] Recently, Carr *et al.* investigated monovalent, divalent, and trivalent ion adsorption on GO films using XR and VSFG.[32] The $q_{max}$ for the XR data was 0.55 Å$^{-1}$, which gives a resolution of 6 Å. The spreading solution volume was 1 mL.

This work reports a simple and effective method to prepare GO films at the air/water interface by sonicating and filtering the GO spreading solution, which is then placed on a subphase *via* dropwise addition with a micro syringe (Fig. 1). This process decreases the total GO spreading volume to ∼100 μL, a 10–100× improvement *versus* prior studies, thus significantly reducing GO dissolution and decreasing the thin film prep time to a few minutes. The versatility of the method is demonstrated by preparing and characterizing films from different commercial GO solutions. The resulting films are high quality, *i.e.* very smooth and uniform, and allow XR measurements up to $q_{max} =$ 0.7 Å$^{-1}$, with a resolution of 4.5 Å. The high quality of the GO films also facilitates observation of a new water population, *via* VSFG, that primarily interacts with the GO film. This water population has not been observed in previous studies at the air/

water interface[17,32] and highlights the importance of both the GO composition and film preparation on understanding nanoscale water structure and ion interactions.

## 2 Experimental methods

### 2.1 Materials and sample preparation

Three different graphene oxide samples were obtained: GO-1 (1 mg mL$^{-1}$ graphene oxide, 15–20 sheets, oxygen content ≤11%, Sigma-Aldrich, USA); GO-2 (2 mg mL$^{-1}$ carboxyl-enriched graphene oxide, 15–20 sheets, oxygen content 45–50%, Sigma-Aldrich, USA); and GO-3 (10 mg mL$^{-1}$ graphene oxide, 3–5 sheets, oxygen content 40–50%, Standard Graphene, South Korea). Other chemicals were purchased from Sigma-Aldrich, USA and used without further purification. Yttrium chloride solutions were prepared with yttrium(III) chloride hexahydrate (99.99% purity) and ultrapure water with resistivity of 18.2 MΩ cm (Millipore, Synergy Water Purification System). Further details are discussed in the Results and discussion.

### 2.2 Synchrotron X-ray experiments

X-ray fluorescence near total reflection (XFNTR) and X-ray reflectivity (XR) experiments were completed at sector 15-ID-C, NSF's ChemMatCARS, of the Advanced Photon Source at Argonne National Laboratory. All data were collected using an incident X-ray energy of 18.3 keV and motorized slits set the beam size to 2 mm × 0.02 mm, horizontally and vertically, respectively. We prepared GO samples on a Langmuir trough and purged the sample chamber with helium to reduce background scattering and mitigate beam damage. The local surface pressure of each GO film was 20 mN m$^{-1}$, as controlled by the Langmuir trough, expect for the unfiltered sample, which reached a maximum surface pressure of 4 mN m$^{-1}$.

### 2.3 XFNTR experiments

XFNTR data were collected on a Vortex-60EX multi-cathode energy dispersive detector mounted approximately 10 mm above the sample surface. We measured the fluorescence intensity of the $K_{\alpha 1}$ edge for Y as a function of momentum transfer $q_Z = (4\pi/\lambda)\sin(2\theta/2)$, where $\lambda$ is the X-ray wavelength and $\theta$ is the incident beam angle, around the critical angle $q_C$, the angle at which the X-rays undergo total external reflection. Data were fitted using the computed total illuminated volume and varied surface ion concentration by minimizing the total sum of squares, as detailed elsewhere.[33]

### 2.4 XR experiments

Specular XR data were collected on a 200K Pilatus detector as a function of $q_Z$. The sample was shifted periodically to avoid beam damage. We fitted the XR data using slab model by minimizing the total sum of squares *via* a Parratt formalism to determine slab thickness, roughness, and electron density, as described previously in detail. Because the roughness of each slab is typically dominated by surface capillary waves, all roughness values for each sample were forced to be equal.[34,35] Data were fitted using StochFit.[35]
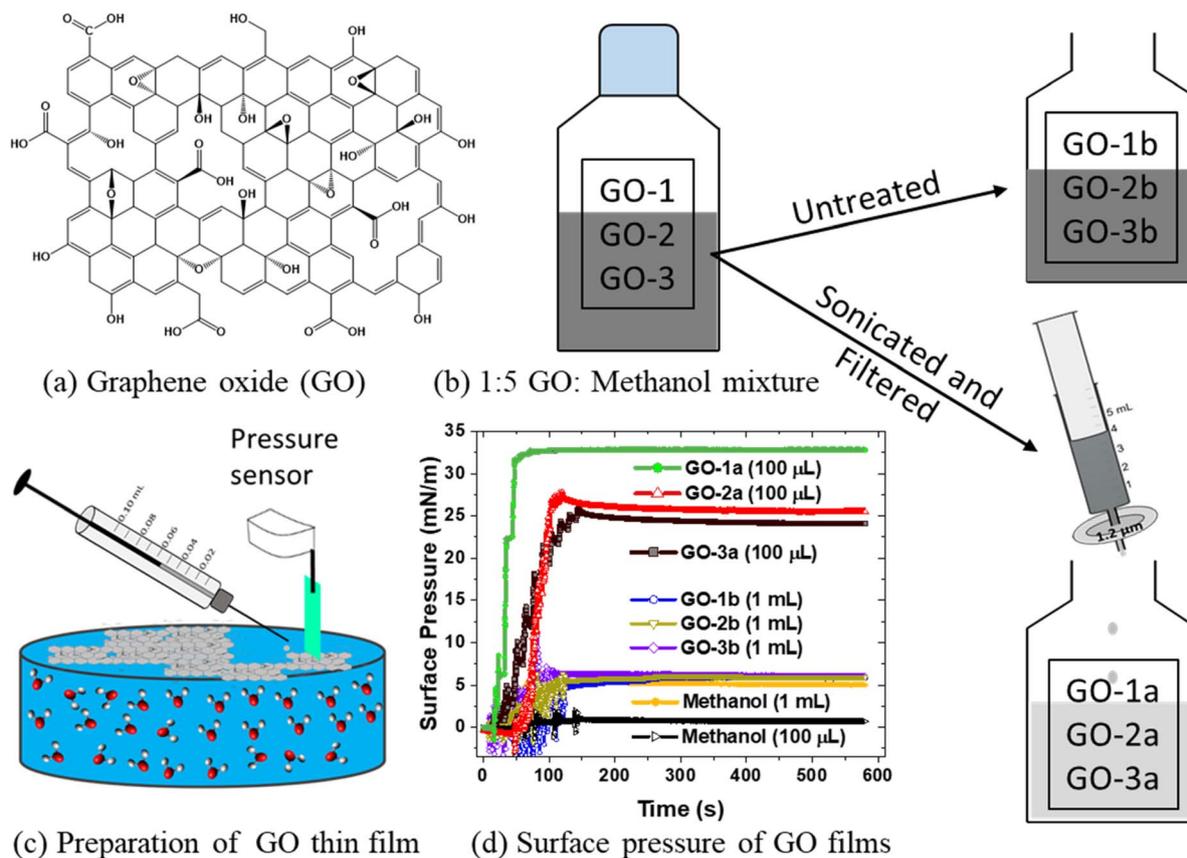
**Fig. 1** (a) Representative structure of the graphene oxide (GO). (b) 1 mg mL$^{-1}$ aqueous GO suspensions (GO-1, GO-2, and GO-3) are diluted with a methanol/water mixture (1 : 5, v/v). Samples were then sonicated for an hour and filtered using a 1.2 μm syringe filter to create GO-1a, GO-2a, and GO-3a. Untreated samples are labelled as GO-1b, GO-2b, and GO-3b. (c) GO thin films were prepared in a PTFE dish by spreading 100 μL of GO spreading solution. The surface pressure was measured using a NIMA pressure sensor with a chromatography paper as a Wilhelmy plate. (d) Surface pressure of different GO samples and pure methanol at the air/water interface over time.

### 2.5   VSFG experiments

The VSFG measurements are acquired using an EKSPLA laser system, which has been described previously.[36–40] Briefly, the setup consists of a picosecond laser system, a harmonic unit, an optical parametric generator with difference frequency generation, a spectrometer and a photomultiplier tube detector connected to a monochromator. An amplified Nd:YAG laser system produces 29 ps pulses having 40 mJ energy centered at 1064 nm with a repetition rate of 50 Hz. The harmonic unit splits the 1064 nm laser, and a portion is passed through a second harmonic crystal to generate two beams of 532 nm. One of the 532 nm beams and the 1064 nm beam are used to generate a narrowband IR pulse tunable from 650–4000 cm$^{-1}$ *via* an optical parametric generator and difference frequency generation. The other 532 nm laser beam passes through an adjustable delay stage and is overlapped spatially and temporarily with the IR beam to generate the sum frequency (SF) signal. The polarization of 532 nm is adjusted with a $\lambda/2$ waveplate, and the IR polarization is adjusted by using computer-controlled motorized mirrors. The SFG signal polarization is selected using a Glan polarizer. The SFG signal is then directed to a monochromator and collected with a photomultiplier tube. The VSFG

spectrometer employs reflection geometry where the incident angles of the visible and IR beams are 60° and 55°, respectively, to the surface normal. The visible light is attenuated to an average energy of 200 μJ and the IR energy is maintained at 100 μJ for all measurements. A motorized piezoelectric rotation stage is used to rotate the sample to avoid beam damage. Each spectrum is collected with a 4 cm$^{-1}$ increment over the range of 2800–3800 cm$^{-1}$ and averaged over 100 laser shots per point. The spectra are collected under SSP polarization combinations and are normalized against the SFG spectrum of a z-cut quartz.

The intensity of the VSFG signal ($I_{\text{VSFG}}$) is proportional to the square of the effective second order non-linear susceptibility $\chi_{\text{eff}}^{(2)}$ of the material interface. The experimentally obtained VSFG data are fitted using the function given in eqn (1)[41–44]

$$I_{\text{VSFG}} \propto \left| \chi_{\text{eff}}^{(2)} \right|^2 \propto$$

$$\left| \chi_{\text{NR}}^{(2)} + \sum_{\nu} \frac{A_{\nu}}{\omega_{\text{IR}} - \omega_{\nu} + i\Gamma_{\nu}} e^{i\varphi_2} + \frac{\kappa}{\sqrt{\kappa^2 + \Delta k_z^2}} e^{i\varphi_3} \chi^{(3)} \Phi_0 \right|^2 \quad (1)$$

where, $\chi_{\text{NR}}^{(2)}$ is the non-resonant component of $\chi^{(2)}$, $A_{\nu}$ is the resonance amplitude, $\omega_{\nu}$ is resonant frequency, $\omega_{\text{IR}}$ is the IR frequency, $\Gamma_{\nu}$ is damping constant of $\nu^{\text{th}}$ vibrational mode

which describes the linewidth of the transition, $\varphi_2$ is the phase, $\kappa$ is the inverse Debye length, $\Delta k_z$ is the inverse SFG coherence length, $\varphi_3$ is the phase angle, $\chi^{(3)}$ is the third order nonlinear susceptibility, and $\varphi_0$ is the surface potential.

The contribution of $\chi^{(3)}$ term to $I_{\text{VSFG}}$ is an active research topic. It has been demonstrated that this term approaches to zero at very low and high ionic strengths.[45,46] Therefore, for simplicity we use a simplified version of the equation for data fitting.

$$I_{\text{VSFG}} \propto \left|\chi_{\text{eff}}^{(2)}\right|^2 \propto \left|\chi_{\text{NR}}^{(2)} + \sum_\nu \frac{A_\nu}{\omega_{\text{IR}} - \omega_\nu + i\Gamma_\nu}e^{i\varphi_2}\right|^2 \quad (2)$$

However, in the discussions we point out the possible contributions from $\chi^{(3)}$ as demonstrated by the concentration dependent data. We make the comparison between the GO films based on 20 mM data, where eqn (2) is valid.

## 2.6 Surface pressure measurements

Surface pressure of the ultra-thin graphene oxide film was measured using a NIMA pressure sensor with chromatography paper as a Wilhelmy plate. For the synchrotron X-ray experiments, GO films were prepared in a Langmuir trough by spreading the GO solution over a larger area and then compressed using a barrier to reach a surface pressure of 20 mN m$^{-1}$, except for GO-3b which reached a maximum surface pressure of 4 mN m$^{-1}$. For VSFG experiments, GO films were prepared in a circular polytetrafluoroethylene (PTFE) dish having a 7 cm inner diameter. 100 μL of each GO suspension is added dropwise by using a 100 μL syringe (Hamilton, USA) in a sample cell containing 25 mL of ultrapure water.

# 3 Results and discussion

To demonstrate the universality of the preparation method, three commercially obtained GO samples were compared: 1 mg mL$^{-1}$ GO (Sigma-Aldrich, USA) (GO-1), 2 mg mL$^{-1}$ carboxyl-enriched GO (Sigma-Aldrich, USA) (GO-2) diluted to 1 mg mL$^{-1}$ with ultra-pure water, and 10 mg mL$^{-1}$ GO (Standard Graphene, South Korea) diluted to 1 mg mL$^{-1}$ with ultra-pure water (GO-3). Each GO solution was diluted in a methanol/water (5 : 1, v/v) mixture to get a final concentration of 0.17 mg mL$^{-1}$. Samples were then sonicated for 1 hour and filtered with a 1.2 μm syringe filter (Fig. 1b). The final solution is slightly lighter in color and less concentrated than the diluted 0.17 mg mL$^{-1}$ solution. The 5 : 1 methanol/water mixture is found to be more effective in dispersing GO in solution and spreading rapidly on the water surface.[16] When GO suspension in methanol is gently added on water surface, it spreads rapidly on the surface that allow GO sheets to remain at the surface.[47] The surface tension of methanol at the interface is much lower than the surface tension of water. Their corresponding surface free energies are $3.53 \times 10^{-21}$ J per molecule for methanol and $7.0 \times 10^{-21}$ J per molecule for water.[48] This helps to spread the GO at the surface quickly before methanol undergoes evaporation. The sonicated and filtered samples are labeled GO-1a, GO-

2a, and GO-3a, and the untreated samples, which are neither sonicated nor filtered, are labeled as GO-1b, GO-2b, and GO-3b (Fig. 1). Dynamic light scattering measurements of the sample using a Malvern Zetasizer Nano give a hydrodynamic diameter of $1.7 \pm 0.3$ μm (GO-1a), $6.0 \pm 0.8$ μm (GO-2a), and $2.6 \pm 0.2$ μm (GO-3a). A comparative study using X-ray photoelectron spectroscopy (XPS) and FTIR measurements were performed for three different GO membranes prepared by vacuum filtration. The carbon/oxygen (C/O) ratios are: 43.1% C/11.3% O = 3.81 for GO-1; 71.4% C/28.2% O = 2.53 for GO-2; and 74.6% C/24.9% O = 3.00 for GO-3, as determined using XPS. The lower the value of C/O ratio, higher the oxygen content in the given film. FTIR measurements also showed the presence of higher oxygen containing functional groups in GO-2 and GO-3 compared to GO-1. See detail in the ESI.†

There are two key steps in this preparation process. First, sonication is completed in the methanol/water mixture. Sonicating only in water does not yield high quality films (data not shown). Second, samples were filtered after sonication. Samples that were sonicated but not filtered did not form good quality films (ESI, Fig. S7†). It reasons that filtering removes any remaining GO aggregates, which prevents the suspended flakes from stacking and allows the flakes to float on the subphase. Both sonication and filtration had been used in previous studies.[17,24,29,32] However, the relatively longer sonication reported here followed by filtering (1.2 μm filter) decreases the amount of spreading solution by 10–100× and forms significantly smoother films, which allows highly sensitive measurements. This method differs compared to the work by Carr et al. in which GO solutions were mixed with methanol and sequentially filtered using 1.2 μm, 0.45 μm, and 0.2 μm syringe filters.[32] Those suspensions were not sonicated and contained notably smaller GO flakes due to the smaller pore size of the filters.[32]

Fig. 1c shows a GO thin film formed in a fixed area by spreading the GO solution with a micro syringe. Fig. 1d shows the measured surface pressure as a function of time during spreading for each solution. Spreading is completed in 100 seconds. The sonicated and filtered samples (GO-1a, GO-2a, GO-3a) reach a high surface pressure after 100 μL solution is spread. GO-2a and GO-3a show a similar trend while GO-1a reaches a higher surface pressure, which will be discussed below. The untreated samples (GO-1b, GO-2b, GO-3b) show very small changes in surface pressure even after ten times more (1 mL) spreading solution was used. Indeed, a control experiment with only 1 mL methanol shows a similar change in the surface pressure, which suggests that the untreated GO does not have a significant presence at the interface and likely dissolved into the subphase.

Fig. 2 shows the VSFG data from –OH and –CH regions of the GO films. The eqn (2) is used to fit the data and the obtained fit parameters are given in the ESI.† The VSFG measurements are taken at pH $\sim$ 6, where $Y^{3+}$ remains in its free ionic form without further speciation to its hydroxide form which usually happens at pH higher than 7.[49,50] The apparent p$K_a$ of carboxylic acid groups for GO at the air/water interface is 4, suggesting almost all of them are deprotonated. All of the high-quality films (GO-1a, GO-2a, and GO-3a) show a strong water band
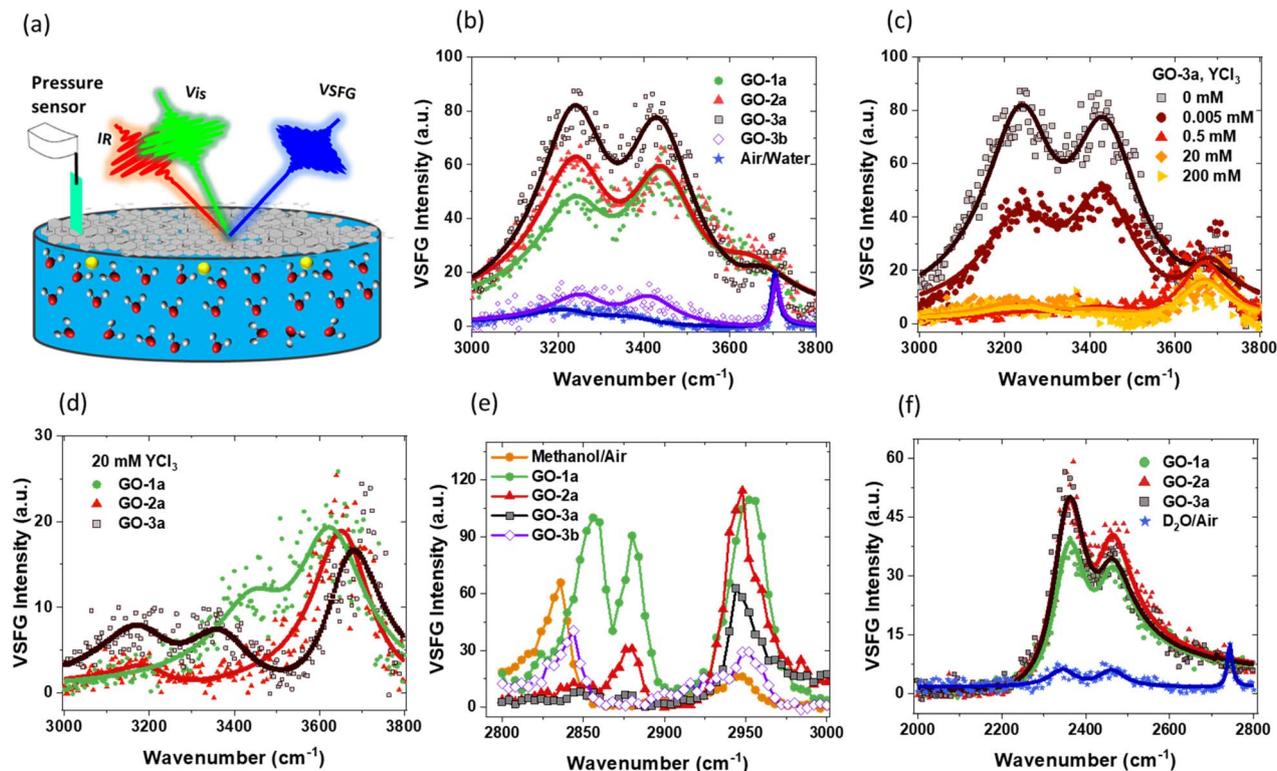
Fig. 2 (a) Schematic showing the VSFG experiments on the GO/aqueous interface. The yellow spheres represent the adsorption of $Y^{3+}$ ions on the GO surface. (b) VSFG intensity of −OH region of different GO films compared to a bare air/water interface. (c) VSFG intensity of the −OH region of GO-3a films on $YCl_3$ subphases with varied concentrations. (d) −OH region of VSFG signal for GO-1a, GO-2a, and GO-3a films on 20 mM $YCl_3$ (e) VSFG intensities of −CH region for various GO films and a bare air/methanol interface. (f) VSFG intensity of the −OD region for different GO films compared to a bare air/$D_2O$ interface. Here, the GO is suspended in a 1 : 5 mixture of $D_2O$ and deuterated methanol ($CD_3OD$).

with three peaks centered at 3250, 3440, and 3640 cm$^{-1}$. The 3250 and 3440 cm$^{-1}$ peaks are typical −OH signals in the presence of surfactants. The 3250 cm$^{-1}$ peak mainly originates from the strongly hydrogen bonded water population oriented by the electric field of the charged film, known as the $\chi^{(3)}$ effect.[51–53] The water population leading to 3440 cm$^{-1}$ peak has weaker hydrogen bonding, is possibly closer to the surface, and might contain water molecules coordinating to the GO films, though this signal is also affected by the surface electric field.

GO-3a has the strongest VSFG signal likely because it has more functional groups per carbon–carbon bond and these groups lead to a stronger electric field. This is supported by the XPS results (Fig. S1–S5†). GO-1a and GO-2a have similar VSFG signals but GO-2a has slightly stronger 3250 cm$^{-1}$ peak, thus agreeing with the supplier information that it is carboxyl-enriched. However, GO-2a still has fewer carboxyl groups compared to GO-3a. It is interesting that the surface pressure for GO-1a was the highest although it has the lowest VSFG signal. The −CH region VSFG data (2800–2900 cm$^{-1}$ band in Fig. 2e) suggest that GO-1a has higher hydrocarbon components possibly from impurities, responsible for the higher surface pressure. The GO solutions utilized were used as received from the suppliers. XPS analysis shows sulfur signal, which is a common contaminate leftover from the GO synthesis (ESI†). This implies other leftover residuals from the synthesis

also remain in the dispersions. Additionally, the GO suppliers purport that no additional surfactants or stabilizers are added to the GO dispersions. The presented film preparation method generates high-quality films regardless of leftover residuals.

The 3640 cm$^{-1}$ (Fig. 2b) peak is too high of a frequency to be a water–water hydrogen bond and is likely from the water population trapped in between the GO layers. Earlier VSFG studies by Carr et al.[32] and Hong et al.[17] at the air/water interface did not observe this 3640 cm$^{-1}$ peak so clearly. Ab initio molecular dynamics (AIMD) studies by David et al. suggest that this peak appears when C/O ratio is low (∼2) and disappears when it is high (∼4).[13] They also did VSFG experiments with spin-coated GO and reduced-GO films on sapphire. However, the sapphire substrate also had a strong peak around 3640 cm$^{-1}$, which obscured the results. Considering that the C/O ratio is about 2–3 for GO-2a and GO-3a samples in this study, it is reasonable to say that the present results support the emergence of an additional VSFG high frequency signal in the water region as suggested computationally by David et al.[13] This analysis is also consistent with the VSFG results reported previously by Carr et al. where the C/O ratio was ∼5 and this high frequency peak was not observed.[32] That study utilized a different thin film preparation procedure. The absence of this high frequency peak in the water region in the Hong et al.[17] study despite having a C/O ratio ∼2 implies that the C/O ratio is

not the only factor affecting the VSFG signal. The present work suggests that the film quality also plays a role in the observation of this peak. The films created using the presented spreading method are more uniform and of higher quality, which makes it possible to detect this distinct water population. We also note that this interpretation does not rule out the possibility of some water molecules forming stronger hydrogen bonds with the functional groups of the GO.

Fig. 2c shows VSFG signal from the –OH region as a function of the subphase $YCl_3$ concentration. As ions adsorb to the GO film, the VSFG signal should decrease, since the adsorbed ions disrupt water organization and screen the charge of the film.[54–56] Above 0.5 mM $YCl_3$, the 3250 and 3440 cm$^{-1}$ peaks decrease significantly but 3640 cm$^{-1}$ peak stays unchanged, which supports the hypothesis that this signal originates from water molecules in between the GO layers and is thus minimally affected by the adsorbed ions and the diminishing electric field. At 20 mM, GO-3a still has some 3250 and 3440 cm$^{-1}$ signal, probably due to functional groups that are inaccessible to adsorbed ions but can create a local electric field (zoomed in version is shown in Fig. S9†). GO-1a and GO-2a samples show a similar trend (data not shown).

VSFG data for GO films created on concentrated subphases more relevant to GO membrane applications are shown in Fig. 2d. All samples show very similar 3640 cm$^{-1}$ signal, which suggests that the preparation method presented creates similar films even though the GO solutions were obtained from different vendors. The 3250 and 3440 cm$^{-1}$ peaks are clearly different between the samples. These peaks are mostly absent in GO-2a, consistent with the XPS and previous VSFG results that suggest GO-2a has fewer functional groups per C–C bond. GO-3a retains the strongest signal, which supports the prior interpretation that some functional groups may be inaccessible to ions but their local interactions with water molecules can cause the VSFG signal *via* orientational ordering of water molecules. Understanding the true origin of these differences requires more detailed investigations. The goal of this work is to demonstrate multiple examples of the advantages of high-quality GO films. The improved film quality allows detection of subtle differences that can later be compared to computational studies and correlated with membrane applications.

The interpretation of –OH region SFG signal has been an active debate topic due to multiple factors that may possibly contribute to the signal. In the presence of a fixed electric field, absorptive and dispersive contributions can mix, making it important to include interfacial potential-dependent $\chi^{(3)}$ term explicitly (eqn (1)). However, it is known that the factor in front of $\chi^{(3)}$ approaches to zero at high ionic strengths and the overall SFG signal is dominated by the $\chi^{(2)}$ term.[45] Therefore, the SFG signal at high ionic strength, which is dominated by 3600 cm$^{-1}$ peak (Fig. 2d), can be considered as it is without any $\chi^{(3)}$ contribution. This is consistent with recent studies demonstrating that the $|\chi^{(3)}|$ is centered around 3200 cm$^{-1}$.[45]

VSFG can provide information about interfacial chemical signatures.[57] The measurements studying free methanol/air interface and GO films prepared in methanol show that no methanol is present at the interface for the high quality films (Fig. 2e). However, the low-quality film shows signature of methanol (Fig. 2e), possibly due to the large volume of the spreading solution (1 mL). These data show the importance of preparing high-quality films with a minimum volume of spreading solution.

The –OH region of VSFG signal may have contributions from –OH groups on GO film and from the surrounding water. To clarify, GO samples in deuterated methanol were prepared with and spread on $D_2O$. The results show that there is no detectable –OH signal from GO films under these conditions (Fig. S8a†). However, the VSFG –OD region (Fig. 2f) shows interesting differences compared to –OH region (Fig. 2b). First, the expected high frequency peak around 2700 cm$^{-1}$, *i.e.* the deuterated 3640 cm$^{-1}$ peak analogue, is completely missing. Second, the VSFG intensity of GO-2a and GO-3a are more similar in contrast to –OH region, where the GO-3a VSFG signal is significantly higher. These results broadly suggest that $D_2O$ and $H_2O$ interact differently with GO films. Indeed, recent studies demonstrated that GO membranes can be used for isotopic water separations.[58,59] The high-quality films prepared in this study allow one to observe clear differences between the interactions of $D_2O$ and $H_2O$ with GO, which provides new opportunities to understand the fundamental interactions underlying isotopic water selectivity of GO.

While VSFG gives direct information about the interfacial water structure, it only gives indirect information on the film structure and ion adsorption. To obtain direct information about the film and ion adsorption, synchrotron X-ray reflectivity (XR) and X-ray fluorescence near total reflection (XFNTR) experiments were conducted at Sector 15 ID-C of Advanced Photon Source (Fig. 3).[34,60] For these experiments, GO films were prepared in a Langmuir trough by spreading the GO solution over a larger area and then compressing the barrier to reach a surface pressure of 20 mN m$^{-1}$.

XFNTR can directly quantify the number of adsorbed ions at the interface.[34] The element-specific fluorescence emission signal of Y ($K_{\alpha1}$, 14.958 keV) was recorded as a function of the incidence angle below and above the critical angle (Fig. 3a and b). Because the refractive index of water for X-rays is less than 1, X-rays undergo total external reflection below the critical angle ($q_c$). Only the evanescent waves penetrate a few nanometers near the interface, which allows quantification of the total number of yttrium ions in this region. Fluorescence signal measured at $q_z < q_c$ is generated by ions at the interface while signal measured at $q_z$ greater than the critical angle stems from ions at the interface and in the bulk. Quantitative fitting[34] of the XFNTR data for GO-3a and GO-2a films on 0.5 mM $YCl_3$ subphases give coverages of 1 $Y^{3+}$ ion per 199 $\pm$ 4 Å$^2$ and 434 $\pm$ 19 Å$^2$, respectively, meaning more $Y^{3+}$ absorbs to GO-3a *versus* GO-2a. These results broadly agree with VSFG and XPS results discussed before, which show that GO-3a has higher surface charge and more carboxyl groups per carbon–carbon bond. The number of carboxyl groups is not the only factor in ion adsorption, as not all functional groups may be available to interact with the subphase due to the structural organization of the GO film and ions may adsorb on other defect sites or functional groups.
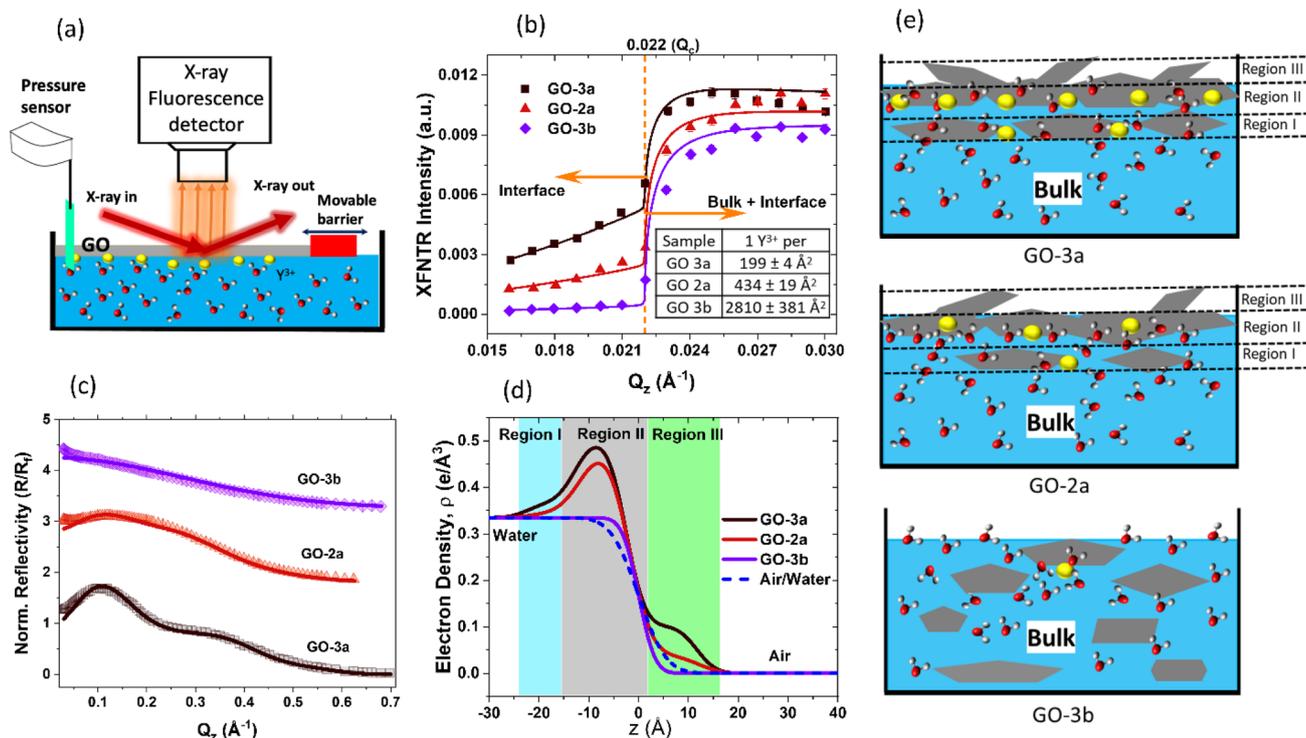
Fig. 3 (a) Schematic showing X-ray fluorescence near total reflection (XFNTR) and X-ray reflectivity (XR) measurements of GO films at air/aqueous interface. The GO films were compressed to 20 mN m$^{-1}$, except for GO-3b which reached a maximum surface pressure of 4 mN m$^{-1}$. The yellow spheres represent the adsorption of Y$^{3+}$ ions on the GO surface. (b) XFNTR intensity plotted over momentum transfer $Q_z$ for different GO films each prepared on a 0.5 mM YCl$_3$ subphase. Error bars are derived from experimental counting statistics. Inset table shows the density of Y$^{3+}$ ions adsorbed to the GO films obtained by fitting the XFNTR data. (c) Normalized XR intensity (symbols) plotted over momentum transfer $Q_z$ for different GO films. The data are vertically offset for clarity. Solid lines show the fits to the data. (d) Calculated electron density profile as a function of distance from the interface ($Z$) for different GO films prepared on 0.5 mM YCl$_3$ subphases compared to the electron density profile of an ideal air/water interface without GO. (e) Cartoons showing possible adsorption of Y$^{3+}$ ions on GO films with different structures.

To understand the interfacial film structure, XR experiments were conducted. XR records the specularly reflected X-ray intensity from the air/water interface as a function of the incident angle $\theta$, which is related to the vertical momentum transfer via $q_z = \frac{4\pi}{\lambda}\sin\left(\frac{2\theta}{2}\right)$. Fig. 3c shows the XR data (symbols) and fits (solid lines), and the electron density profiles derived from them are shown in Fig. 3d, which were calculated using a Parratt formalism.[34,35] A three-layer model is necessary to fit GO-3a data, which shows clear oscillations due to the layered structure of the film (Fig. 3c). The oscillations are less pronounced for GO-2a, which suggests a lower electron density contrast or a lower quality film. GO-3b does not require any boxes and only interfacial roughness parameter was fit. The obtained fit parameters and the comparison of fit models with different box numbers are given in the ESI.† It is important to note that in a lower resolution experiment these three layers may appear as a single layer.

The major results of the XR measurements can be understood from the Fresnel normalized data in Fig. 3c. At a simple interface transitioning from water to air, XR data looks featureless. GO-3b (Purple) is a good example. Therefore, we can fit that data with a single surface roughness parameter. The resulting electron density profile in Fig. 3d, purple, shows that

there is no significant GO at the interface, but the interfacial roughness is slightly higher than the ideal air/water interface shown by the dashed lines. For GO-2a (red) and GO-3a (black), XR intensity starts increasing over 100% reflection, which is only possible with the constructive interference due to a high density film at the interface.

Both GO-2a and GO-3a have a 1.5 nm main layer, labeled region II in Fig. 3d and e. Considering that a hydrated GO layer is approximately 1 nm thick, this core region likely consists of 1–2 layers. There is also additional material below and above this main layer, labelled as regions I and III, respectively. These regions may be due to tilted GO flakes or extra GO layers. In GO-3a, the electron density of these extra layers is significantly higher compared to the corresponding layers in GO-2a. There may be several reasons for this. First, there is more Y$^{3+}$ adsorption on GO-3a, which increases the overall electron density and XR intensity. As shown above with VSFG of CH-region and the surface pressure measurements, there is also more hydrocarbon components from impurities in GO-2a, which likely dilutes the real GO flake density in the film. XR data support these results and show that GO-3a possibly has thicker, multilayer GO flakes on average compared to GO-2a. Finally, the low-quality GO-3b sample did not form a distinguishable film, as expected (Fig. 3c–e). Taken together, these

    

XFNTR and XR reveal important differences between seemingly similar GO products and show the importance of creating high-quality GO films for detailed, nanoscale analysis.

We name the GO films "ultra-thin" in comparison to the majority of the studies in the literature. Most studies use spin coating, or similar methods, which provide ~100 nm or thicker films. As it is clear from the electron density profiles obtained from the XR data (Fig. 3d), the majority of GO-2a and GO-3a films are indeed ~1.5 nm-thick region II. The region I and III, are detectable due to the high quality and the smoothness of the film. They would be undetectable/ignored in a typical AFM measurement.

## 4  Conclusions

In summary, this paper reported a simple but effective method to prepare ultra-thin GO films at the air/water interface and compared GO films created from dispersions obtained from three different vendors. The high-quality films at the air/water interface, free from substrate effects, allowed clear observation of nanoscale differences between the films. This method paves the way for future studies to elucidate the complex separation mechanisms underpinning GO membrane success. Three water bands were observed in VSFG experiments, including a high frequency band that has not been clearly observed in previous studies[17,32] but has been predicted in AIMD works.[13] These VSFG signals have different origins. The 3250 and 3440 $cm^{-1}$ bands are due to water alignment generated from the surface charge of the GO film while the high frequency 3640 $cm^{-1}$ peak is from water molecules that are directly coordinated to the GO film. The higher quality ultra-thin films created here facilitated observation of this high frequency peak, which appears to be insensitive to ion adsorption. Interestingly, this peak cannot be observed in $D_2O$ experiments, which might be important for future isotope separations studies. Additional XR data revealed the structure of the GO films and XFNTR data demonstrated improved trivalent ion adsorption for the high-quality films. These experiments provide a consistent method to create GO films at the air/water interface, which can be utilized in a variety of future investigations. We note that while this manuscript was under review, our group utilized this high-quality film preparation method to understand the impact of subphase pH on interfacial film properties and rare earth separations in another work.[61] Finally, the complementary use of X-ray and VSFG experiments in a single study provided a detailed picture, which cannot be obtained by a single method.[56,62,63]

## Author contributions

The manuscript was written through contributions of all authors. All authors have given approval to the final version of the manuscript.

## Conflicts of interest

The authors declare no competing interest.

## References

1 B. Mi, Graphene Oxide Membranes for Ionic and Molecular Sieving, *Science*, 2014, **343**, 740–742.

2 R. K. Joshi, P. Carbone, F. C. Wang, V. G. Kravets, Y. Su, I. V. Grigorieva, H. A. Wu, A. K. Geim and R. R. Nair, Precise and Ultrafast Molecular Sieving through Graphene Oxide Membranes, *Science*, 2014, **343**, 752–754.

3 Q. Yang, Y. Su, C. Chi, C. T. Cherian, K. Huang, V. G. Kravets, F. C. Wang, J. C. Zhang, A. Pratt, A. N. Grigorenko, F. Guinea, A. K. Geim and R. R. Nair, Ultrathin Graphene-Based Membrane with Precise Molecular Sieving and Ultrafast Solvent Permeation, *Nat. Mater.*, 2017, **16**, 1198–1202.

4 S. Xue, C. Ji, M. D. Kowal, J. C. Molas, C. W. Lin, B. T. McVerry, C. L. Turner, W. H. Mak, M. Anderson, M. Muni, E. M. V. Hoek, Z. L. Xu and R. B. Kaner, Nanostructured Graphene Oxide Composite Membranes with Ultrapermeability and Mechanical Robustness, *Nano Lett.*, 2020, **20**, 2209–2218.

5 C. Thamaraiselvan, J. B. Wang, D. K. James, P. Narkhede, S. P. Singh, D. Jassby, J. M. Tour and C. J. Arnusch, Laser-Induced Graphene and Carbon Nanotubes as Conductive Carbon-Based Materials in Environmental Technology, *Mater. Today*, 2020, **34**, 115–131.

6 G. Zhang, L. Lin, W. Shen, X. Wang, Y. Wang, L. Cao and F. Liu, A New Strategy for Highly Efficient Separation between Monovalent Cations by Applying Opposite-Oriented Pressure and Electric Fields, *Small*, 2022, **18**, e2203396.

7 J. Luo, L. Yang, D. Sun, Z. Gao, K. Jiao and J. Zhang, Graphene Oxide "Surfactant"-Directed Tunable Concentration of Graphene Dispersion, *Small*, 2020, **16**, e2003426.

8 I. Chandio, F. A. Janjhi, A. A. Memon, S. Memon, Z. Ali, K. H. Thebo, A. A. A. Pirzado, A. A. Hakro and W. S. Khan, Ultrafast Ionic and Molecular Sieving through Graphene

Oxide Based Composite Membranes, *Desalination*, 2021, **500**, 114848.

9  F. Ahmed Janjhi, I. Chandio, A. Ali Memon, Z. Ahmed, K. Hussain Thebo, A. Ali Ayaz Pirzado, A. Ali Hakro and M. Iqbal, Functionalized Graphene Oxide Based Membranes for Ultrafast Molecular Separation, *Sep. Purif. Technol.*, 2021, **274**, 117969.

10  Q. Zhang, X. Qian, K. H. Thebo, H.-M. Cheng and W. Ren, Controlling Reduction Degree of Graphene Oxide Membranes for Improved Water Permeance, *Sci. Bull.*, 2018, **63**, 788–794.

11  T. Foller, L. Madauss, D. Ji, X. Ren, K. K. H. De Silva, T. Musso, M. Yoshimura, H. Lebius, A. Benyagoub, P. V. Kumar, M. Schleberger and R. Joshi, Mass Transport *Via* in-Plane Nanopores in Graphene Oxide Membranes, *Nano Lett.*, 2022, **22**, 4941–4948.

12  S. Tan, D. Zhang, M. T. Nguyen, V. Shutthanandan, T. Varga, R. Rousseau, G. E. Johnson, V. A. Glezakou and V. Prabhakaran, Tuning the Charge and Hydrophobicity of Graphene Oxide Membranes by Functionalization with Ionic Liquids at Epoxide Sites, *ACS Appl. Mater. Interfaces*, 2022, **14**, 19031–19042.

13  R. David, A. Tuladhar, L. Zhang, C. Arges and R. Kumar, Effect of Oxidation Level on the Interfacial Water at the Graphene Oxide-Water Interface: From Spectroscopic Signatures to Hydrogen-Bonding Environment, *J. Phys. Chem. B*, 2020, **124**, 8167–8178.

14  A. J. Carr, S. E. Lee and A. Uysal, Ion and Water Adsorption to Graphene and Graphene Oxide Surfaces, *Nanoscale*, 2023, **15**, 14319–14337.

15  J. Kim, L. J. Cote, F. Kim, W. Yuan, K. R. Shull and J. Huang, Graphene Oxide Sheets at Interfaces, *J. Am. Chem. Soc.*, 2010, **132**, 8180–8186.

16  L. J. Cote, F. Kim and J. Huang, Langmuir-Blodgett Assembly of Graphite Oxide Single Layers, *J. Am. Chem. Soc.*, 2009, **131**, 1043–1049.

17  Y. Hong, J. He, C. Zhang and X. Wang, Probing the Structure of Water at the Interface with Graphene Oxide Using Sum Frequency Generation Vibrational Spectroscopy, *J. Phys. Chem. C*, 2022, **126**, 1471–1480.

18  C. Valtierrez-Gaytan, I. Ismail, C. Macosko and B. L. Stottrup, Interfacial Activity of Graphene Oxide: Anisotropy, Loading Efficiency and Ph-Tunability, *Colloids Surf., A*, 2017, **529**, 434–442.

19  O. C. Compton and S. T. Nguyen, Graphene Oxide, Highly Reduced Graphene Oxide, and Graphene: Versatile Building Blocks for Carbon-Based Materials, *Small*, 2010, **6**, 711–723.

20  S. E. Lee, A. J. Carr, R. R. Kumal and A. Uysal, Monovalent ion–graphene oxide interactions are controlled by carboxylic acid groups: Sum frequency generation spectroscopy studies, *J. Chem. Phys.*, 2024, **160**, 084707.

21  M. Krueger, S. Berg, D. A. Stone, E. Strelcov, D. A. Dikin, J. Kim, L. J. Cote, J. Huang and A. Kolmakov, Drop-Casted Self-Assembling Graphene Oxide Membranes for Scanning Electron Microscopy on Wet and Dense Gaseous Samples, *ACS Nano*, 2011, **5**, 10047–10054.

22  W. S. Chong, S. X. Gan, H. M. Al-Tuwirit, W. Y. Chong, C. S. Lim and H. Ahmad, Nanolitre Solution Drop-Casting for Selective Area Graphene Oxide Coating on Planar Surfaces, *Mater. Chem. Phys.*, 2020, **249**, 122970.

23  C. A. Amadei and C. D. Vecitis, How to Increase the Signal-to-Noise Ratio of Graphene Oxide Membrane Research, *J. Phys. Chem. Lett.*, 2016, **7**, 3791–3797.

24  N. Bonatout, F. Muller, P. Fontaine, I. Gascon, O. Konovalov and M. Goldmann, How Exfoliated Graphene Oxide Nanosheets Organize at the Water Interface: Evidence for a Spontaneous Bilayer Self-Assembly, *Nanoscale*, 2017, **9**, 12543–12548.

25  T. M. McCoy, A. J. Armstrong, J. E. Moore, S. A. Holt, R. F. Tabor and A. F. Routh, Spontaneous Surface Adsorption of Aqueous Graphene Oxide by Synergy with Surfactants, *Phys. Chem. Chem. Phys.*, 2022, **24**, 797–806.

26  F. Kim, L. J. Cote and J. Huang, Graphene Oxide: Surface Activity and Two-Dimensional Assembly, *Adv. Mater.*, 2010, **22**, 1954–1958.

27  H. L. Nie, X. Dou, Z. Tang, H. D. Jang and J. Huang, High-Yield Spreading of Water-Miscible Solvents on Water for Langmuir-Blodgett Assembly, *J. Am. Chem. Soc.*, 2015, **137**, 10683–10688.

28  M. A. Creighton, Y. Ohata, J. Miyawaki, A. Bose and R. H. Hurt, Two-Dimensional Materials as Emulsion Stabilizers: Interfacial Thermodynamics and Molecular Barrier Properties, *Langmuir*, 2014, **30**, 3687–3696.

29  D. López-Díaz, M. D. Merchan, M. M. Velazquez and A. Maestro, Understanding the Role of Oxidative Debris on the Structure of Graphene Oxide Films at the Air-Water Interface: A Neutron Reflectivity Study, *ACS Appl. Mater. Interfaces*, 2020, **12**, 25453–25463.

30  A. M. Dimiev and T. A. Polson, Contesting the Two-Component Structural Model of Graphene Oxide and Reexamining the Chemistry of Graphene Oxide in Basic Media, *Carbon*, 2015, **93**, 544–554.

31  Z. Guo, S. Wang, G. Wang, Z. Niu, J. Yang and W. Wu, Effect of Oxidation Debris on Spectroscopic and Macroscopic Properties of Graphene Oxide, *Carbon*, 2014, **76**, 203–211.

32  A. J. Carr, R. R. Kumal, W. Bu and A. Uysal, Effects of Ion Adsorption on Graphene Oxide Films and Interfacial Water Structure: A Molecular-Scale Description, *Carbon*, 2022, **195**, 131–140.

33  M. Bonn, Y. Nagata and E. H. Backus, Molecular Structure and Dynamics of Water at the Water-Air Interface Studied with Surface-Specific Vibrational Spectroscopy, *Angew. Chem., Int. Ed.*, 2015, **54**, 5560–5576.

34  M. K. Bera, W. Bu and A. Uysal, Liquid Surface X-Ray Scattering, in *Physical Chemistry of Gas-Liquid Interfaces*, ed. J. Faust and J. House, Elsevier, 2018, pp. 167–194.

35  S. M. Danauskas, D. X. Li, M. Meron, B. H. Lin and K. Y. C. Lee, Stochastic Fitting of Specular X-Ray Reflectivity Data Using Stochfit, *J. Appl. Crystallogr.*, 2008, **41**, 1187–1193.

36  K. Lovering, S. Nayak, W. Bu and A. Uysal, The Role of Specific Ion Effects in Ion Transport: The Case of Nitrate and Thiocyanate, *J. Phys. Chem. C*, 2019, **124**, 573–581.

37 W. Rock, B. Qiao, T. Zhou, A. E. Clark and A. Uysal, Heavy Anionic Complex Creates a Unique Water Structure at a Soft Charged Interface, *J. Phys. Chem. C*, 2018, **122**, 29228–29236.

38 S. Nayak, R. R. Kumal, Z. Liu, B. Qiao, A. E. Clark and A. Uysal, Origins of Clustering of Metalate-Extractant Complexes in Liquid–Liquid Extraction, *ACS Appl. Mater. Interfaces*, 2021, **13**, 24194–24206.

39 R. R. Kumal, P. N. Wimalasiri, M. J. Servis and A. Uysal, Thiocyanate Ions Form Antiparallel Populations at the Concentrated Electrolyte/Charged Surfactant Interface, *J. Phys. Chem. Lett.*, 2022, **13**, 5081–5087.

40 S. Nayak, R. R. Kumal and A. Uysal, Spontaneous and Ion-Specific Formation of Inverted Bilayers at Air/Aqueous Interface, *Langmuir*, 2022, **38**, 5617–5625.

41 X. Zhuang, P. B. Miranda, D. Kim and Y. R. Shen, Mapping Molecular Orientation and Conformation at Interfaces by Surface Nonlinear Optics, *Phys. Rev. B: Condens. Matter Mater. Phys.*, 1999, **59**, 12632–12640.

42 D. Verreault, W. Hua and H. C. Allen, From Conventional to Phase-Sensitive Vibrational Sum Frequency Generation Spectroscopy: Probing Water Organization at Aqueous Interfaces, *J. Phys. Chem. Lett.*, 2012, **3**, 3012–3028.

43 A. G. Lambert, P. B. Davies and D. J. Neivandt, Implementing the Theory of Sum Frequency Generation Vibrational Spectroscopy: A Tutorial Review, *Appl. Spectrosc. Rev.*, 2005, **40**, 103–145.

44 I. V. Stiopkin, H. D. Jayathilake, A. N. Bordenyuk and A. V. Benderskii, Heterodyne-Detected Vibrational Sum Frequency Generation Spectroscopy, *J. Am. Chem. Soc.*, 2008, **130**, 2271–2275.

45 J. Hunger, J. Schaefer, P. Ober, T. Seki, Y. Wang, L. Prädel, Y. Nagata, M. Bonn, D. J. Bonthuis and E. H. G. Backus, Nature of Cations Critically Affects Water at the Negatively Charged Silica Interface, *J. Am. Chem. Soc.*, 2022, **144**, 19726–19738.

46 A. J. Carr, S. E. Lee and A. Uysal, Heavy *Versus* Light Lanthanide Selectivity for Graphene Oxide Films Is Concentration-Dependent, *J. Phys. Chem. C*, 2023, **127**, 14363–14373.

47 L. J. Cote, J. Kim, V. C. Tung, J. Luo, F. Kim and J. Huang, Graphene Oxide as Surfactant Sheets, *Pure Appl. Chem.*, 2010, **83**, 95–110.

48 K. R. Wilson, R. D. Schaller, D. T. Co, R. J. Saykally, B. S. Rude, T. Catalano and J. D. Bozek, Surface Relaxation in Liquid Water and Methanol Studied by X-Ray Absorption Spectroscopy, *J. Chem. Phys.*, 2002, **117**, 7738–7744.

49 F. Raji, M. Ejtemaei and A. V. Nguyen, Resolving the Mystery of the Second Charge Reversal on Solid Surfaces in the Presence of Divalent Heavy Metal Ions, *Appl. Surf. Sci.*, 2020, **529**, 147128.

50 A. Sthoer, E. M. Adams, S. Sengupta, R. W. Corkery, H. C. Allen and E. C. Tyrode, La3+ and Y3+ Interactions with the Carboxylic Acid Moiety at the Liquid/Vapor Interface: Identification of Binding Complexes, Charge

Reversal, and Detection Limits, *J. Colloid Interface Sci.*, 2022, **608**, 2169–2180.

51 A. Tuladhar, S. M. Piontek, L. Frazer and E. Borguet, Effect of Halide Anions on the Structure and Dynamics of Water Next to an Alumina (0001) Surface, *J. Phys. Chem. C*, 2018, **122**, 12819–12830.

52 P. E. Ohno, H. F. Wang and F. M. Geiger, Second-Order Spectral Lineshapes from Charged Interfaces, *Nat. Commun.*, 2017, **8**, 1032.

53 X. Chen, W. Hua, Z. Huang and H. C. Allen, Interfacial Water Structure Associated with Phospholipid Membranes Studied by Phase-Sensitive Vibrational Sum Frequency Generation Spectroscopy, *J. Am. Chem. Soc.*, 2010, **132**, 11336–11342.

54 K. C. Jena, P. A. Covert and D. K. Hore, The Effect of Salt on the Water Structure at a Charged Solid Surface: Differentiating Second- and Third-Order Nonlinear Contributions, *J. Phys. Chem. Lett.*, 2011, **2**, 1056–1061.

55 B. Rehl and J. M. Gibbs, Role of Ions on the Surface-Bound Water Structure at the Silica/Water Interface: Identifying the Spectral Signature of Stability, *J. Phys. Chem. Lett.*, 2021, **12**, 2854–2864.

56 R. R. Kumal, S. Nayak, W. Bu and A. Uysal, Chemical Potential Driven Reorganization of Anions between Stern and Diffuse Layers at the Air/Water Interface, *J. Phys. Chem. C*, 2021, **126**(2), 1140–1151.

57 C. M. Johnson and S. Baldelli, Vibrational Sum Frequency Spectroscopy Studies of the Influence of Solutes and Phospholipids at Vapor/Water Interfaces Relevant to Biological and Environmental Systems, *Chem. Rev.*, 2014, **114**, 8416–8446.

58 K. Ching, A. Baker, R. Tanaka, T. Zhao, Z. Su, R. S. Ruoff, C. Zhao and X. Chen, Liquid-Phase Water Isotope Separation Using Graphene-Oxide Membranes, *Carbon*, 2022, **186**, 344–354.

59 A. Mohammadi, M. R. Daymond and A. Docoslis, New Insights into the Structure and Chemical Reduction of Graphene Oxide Membranes for Use in Isotopic Water Separations, *J. Membr. Sci.*, 2022, **659**, 120785.

60 P. S. Pershan and M. Schlossman, *Liquid Surfaces and Interfaces: Synchrotron X-Ray Methods*, Cambridge University Press, 2012.

61 A. J. Carr, S. E. Lee, R. R. Kumal, W. Bu and A. Uysal, Convenient Confinement: Interplay of Solution Conditions and Graphene Oxide Film Structure on Rare Earth Separations, *ACS Appl. Mater. Interfaces*, 2022, **14**, 57133–57143.

62 Y. Horowitz, H. G. Steinruck, H. L. Han, C. Cao, I. I. Abate, Y. Tsao, M. F. Toney and G. A. Somorjai, Fluoroethylene Carbonate Induces Ordered Electrolyte Interface on Silicon and Sapphire Surfaces as Revealed by Sum Frequency Generation Vibrational Spectroscopy and X-Ray Reflectivity, *Nano Lett.*, 2018, **18**, 2105–2111.

63 W. Sung, W. Wang, J. Lee, D. Vaknin and D. Kim, Specificity and Variation of Length Scale over Which Monovalent Halide Ions Neutralize a Charged Interface, *J. Phys. Chem. C*, 2015, **119**, 7130–7137.